Article

Wavefunction matching for solving quantum many-body problems

Serdar Elhatisari[1,2], Lukas Bovermann[3], Yuan-Zhuo Ma[4,5], Evgeny Epelbaum[3], Dillon Frame[6,7], Fabian Hildenbrand[6,7], Myungkuk Kim[8], Youngman Kim[8], Hermann Krebs[3], Timo A. Lähde[6,7], Dean Lee[4✉], Ning Li[9], Bing-Nan Lu[10], Ulf-G. Meißner[2,6,7,11], Gautam Rupak[12], Shihang Shen[6,7], Young-Ho Song[13] & Gianluca Stellin[14]

Ab initio calculations have an essential role in our fundamental understanding of quantum many-body systems across many subfields, from strongly correlated fermions[1–3] to quantum chemistry[4–6] and from atomic and molecular systems[7–9] to nuclear physics[10–14]. One of the primary challenges is to perform accurate calculations for systems where the interactions may be complicated and difficult for the chosen computational method to handle. Here we address the problem by introducing an approach called wavefunction matching. Wavefunction matching transforms the interaction between particles so that the wavefunctions up to some finite range match that of an easily computable interaction. This allows for calculations of systems that would otherwise be impossible owing to problems such as Monte Carlo sign cancellations. We apply the method to lattice Monte Carlo simulations[15,16] of light nuclei, medium-mass nuclei, neutron matter and nuclear matter. We use high-fidelity chiral effective field theory interactions[17,18] and find good agreement with empirical data. These results are accompanied by insights on the nuclear interactions that may help to resolve long-standing challenges in accurately reproducing nuclear binding energies, charge radii and nuclear-matter saturation in ab initio calculations[19,20].

Quantum Monte Carlo simulations are a powerful and efficient ab initio method for describing quantum many-body systems using stochastic processes[1,9,15,16,21–23]. If the Monte Carlo amplitudes are positive, then the computational effort grows only as a low power of the number of particles. For many problems of interest, a simple Hamiltonian H^S can be found that is easily computable using Monte Carlo methods and describes the energies and other observable properties of the many-body system in fair agreement with empirical data[24–27]. However, realistic high-fidelity Hamiltonians usually suffer from severe sign problems with positive and negative contributions cancelling each other so that Monte Carlo calculations become impractical. Here we solve the problem using an approach called wavefunction matching. While keeping the observable physics unchanged, wavefunction matching creates a new high-fidelity Hamiltonian H' such that the two-body wavefunctions up to some finite range match that of a simple Hamiltonian H^S, which is easily computed. This allows for a rapidly converging expansion in powers of the difference $H' - H^S$. Although wavefunction matching can be used with any computational scheme, we focus here on quantum Monte Carlo simulations where the method presents a practical strategy for evading sign oscillations in high-fidelity calculations.

While H^S and H' act on many-body systems, the wavefunction-matching process is done at the two-body level only. For the sake of clarity, we define H^S and H' as containing only two-body interactions. Later we also consider the inclusion of three-body interactions. However, that analysis is separate from wavefunction matching.

A unitary transformation U is a linear transformation that maps normalized orthogonal states to other normalized orthogonal states. Starting from a high-fidelity Hamiltonian H with only two-body interactions, wavefunction matching defines a new Hamiltonian $H' = U^\dagger HU$, where $U^\dagger$ is the Hermitian conjugate of U. The unitary transformation is performed at the two-body level. In each two-body angular momentum channel, the unitary transformation U is active only when the separation distance between two particles is less than some chosen distance R. For the calculations presented here, the value $R = 3.72$ fm is used. The dependence on R is extensively discussed in Supplementary Information.

Let us write $\psi_0(r)$, $\psi'_0(r)$ and $\psi^S_0(r)$ for the two-body ground-state wavefunctions of H, H' and the simple Hamiltonian H^S, respectively. Here r is the distance between the two particles. The transformation U is defined such that $\psi'_0(r)$ is proportional to $\psi^S_0(r)$ for $r < R$. The simple
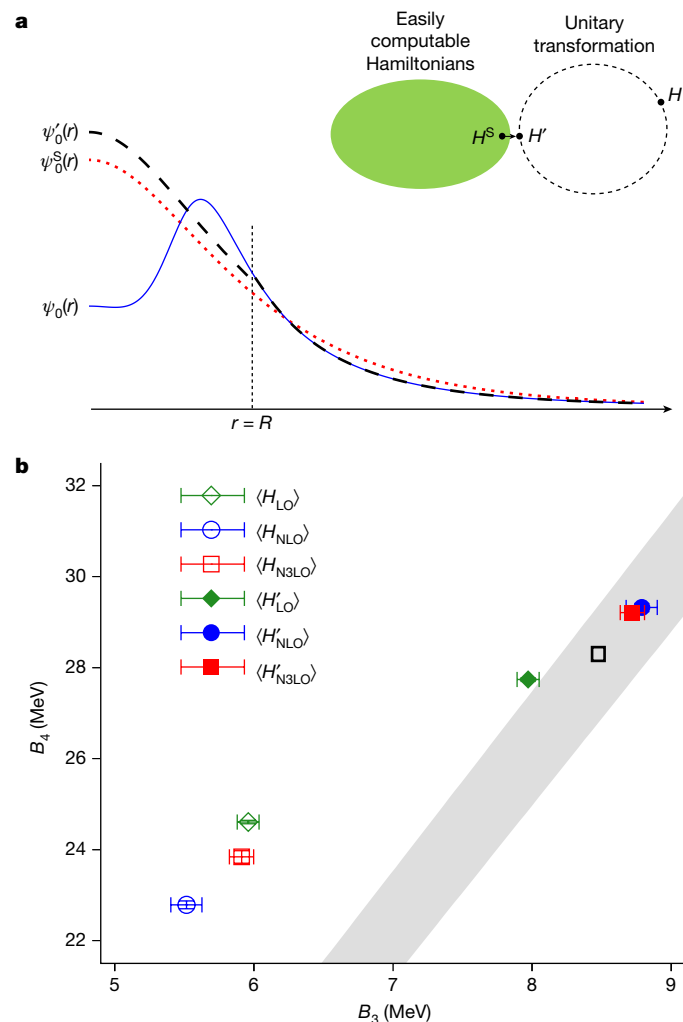
Fig. 1 | Wavefunction matching and the Tjon band. a, Pictorial representation of wavefunction matching. The simple Hamiltonian H^S is an easily computable Hamiltonian whereas the high-fidelity Hamiltonian H is not. A unitary transformation on the two-nucleon interaction with finite range R is used to produce a new Hamiltonian H' that is close to H^S. In each two-body channel, the ground-state wavefunction of H' matches the ground-state wavefunction of H for $r > R$ and is proportional to the ground-state wavefunction of H^S for $r < R$. **b**, The Tjon band correlation between the binding energies of ^{3}H (B_3) and ^{4}He (B_4). The grey band is the predicted result from ref. 31. The black open box shows the empirical point. The green diamond, blue circle and red square points show the results at LO, NLO and N3LO in chiral effective field theory, respectively. The open points show the results from the first-order perturbative calculations using the Hamiltonian H and the filled points are the results of the first-order perturbative calculations using the Hamiltonian H'. The error bars show standard deviations.

Hamiltonian is chosen so that the constant of proportionality is close to 1. For $r > R$, however, U is not active and so $\psi'_0(r)$ remains equal to $\psi_0(r)$. The key point to notice here is that $\psi'_0(r)$ and $\psi^S_0(r)$ are numerically close to each other for all values of r. This can be seen visually in Fig. 1a and is the reason why perturbation theory in powers of $H' - H^S$ converges quickly when starting from low-energy states of H^S.

Wavefunction matching will now be applied to ab initio Monte Carlo nuclear lattice simulations[15,16,25,26,28] using the framework of chiral effective field theory (χEFT)[17,29]. For our realistic Hamiltonian H, we use χEFT two-nucleon interactions at next-to-next-to-next-to-leading order (N3LO) with lattice spacing $a = 1.32$ fm using a low-energy scheme described in Supplementary Information. For our simple Hamiltonian H^S, we use a χEFT interaction at leading order. Details of the interactions

can be found in Supplementary Information. In the following, we use the term 'local' for interactions that do not change the positions of particles and 'non-local' refers to interactions that do change the relative positions of particles. The 'range' of the interaction refers to the separation distance beyond which the interaction between particles becomes negligible.

We calculate all quantities up to first order in perturbation theory, which corresponds to one power in the difference $H' - H^S$. As a first test, we consider the energy of the deuteron, ^{2}H. The wavefunction-matching calculation gives a binding energy of 2.02 MeV, compared with 2.21 MeV for the true binding energy of H and 2.22 MeV for the experimentally observed value. The residual error of 0.1 MeV per nucleon is due to corrections beyond first order in powers of $H' - H^S$. If one does not use wavefunction matching and instead performs the analogous calculation to first order in $H - H^S$, the result is a much less accurate binding energy of 0.68 MeV.

As a second test of wavefunction matching, we calculate the binding energies of ^{3}H and ^{4}He. The Tjon band describes the universal correlations between the ^{3}H and ^{4}He binding energies[30,31]. Provided that there are no long-range non-local interactions, any realistic two-nucleon interaction produces binding energies that lie on the Tjon band. The inclusion of any short-range three-nucleon interaction also preserves this universal relation. In Fig. 1, we show wavefunction-matching calculations using two-nucleon interactions only. At leading order (LO) the calculated point falls outside the Tjon band as the Coulomb interaction is not included, whereas the next-to-leading order (NLO) and N3LO results lie squarely in the middle of the band. We are using a low-energy scheme where the two-nucleon interaction is the same at NLO and next-to-next-to-leading order (NNLO)[32]. The empirical point is also shown in Fig. 1. The good agreement with the Tjon band suggests a residual error of 0.1 MeV per nucleon or less for ^{3}H and ^{4}He. In Supplementary Information, we present numerical evidence that the estimate of 0.1 MeV error per nucleon is also valid for light and medium-mass nuclei. This can be compared with the substantial deviation from the Tjon line if one does not use wavefunction matching and performs the analogous calculation to first order in $H - H^S$. Before proceeding to larger nuclei and many-body systems, we first comment on the current status of ab initio calculations of nuclear structure using χEFT. The following analysis is not directly connected to wavefunction matching. Instead, it is a separate theoretical framework designed to help push beyond the current limitations of ab initio nuclear structure theory.

There has been tremendous progress in the past few years towards producing accurate results for nuclear structure across much of the nuclear chart using a variety of different computational approaches[33–44]. But there is also ample evidence that the calculations are sensitive to the manner in which the short-distance features of the interactions are regulated[20,45–48], a warning sign that systematic errors are not fully under control. Current ab initio calculations have difficulty simultaneously maintaining high-fidelity two-nucleon phase shifts and mixing angles and describing the saturation energy and density of symmetric nuclear matter as well as the binding energies and charge radii of light and medium-mass nuclei. Previous ab initio nuclear structure calculations have either not addressed some of the relevant observables or require further improvement in one or more of these areas. We aim to identify the problem and point to a viable solution.

The results in refs. 49,50 showed that the range and locality of the nuclear interactions have a strong influence on nuclear binding and that the α–α interaction is highly sensitive to the range and locality of the nucleonic interactions as well as omitted higher-order interactions. These same arguments apply to other interactions involving α particles and nucleons. In Supplementary Information, we use the formalism of cluster effective field theory[51–54] for α-particles and nucleons to provide a simple counting argument for the number of parameters that require tuning to reduce unwanted errors. Our strategy is to tune the short-distance features of the three-nucleon interactions to achieve
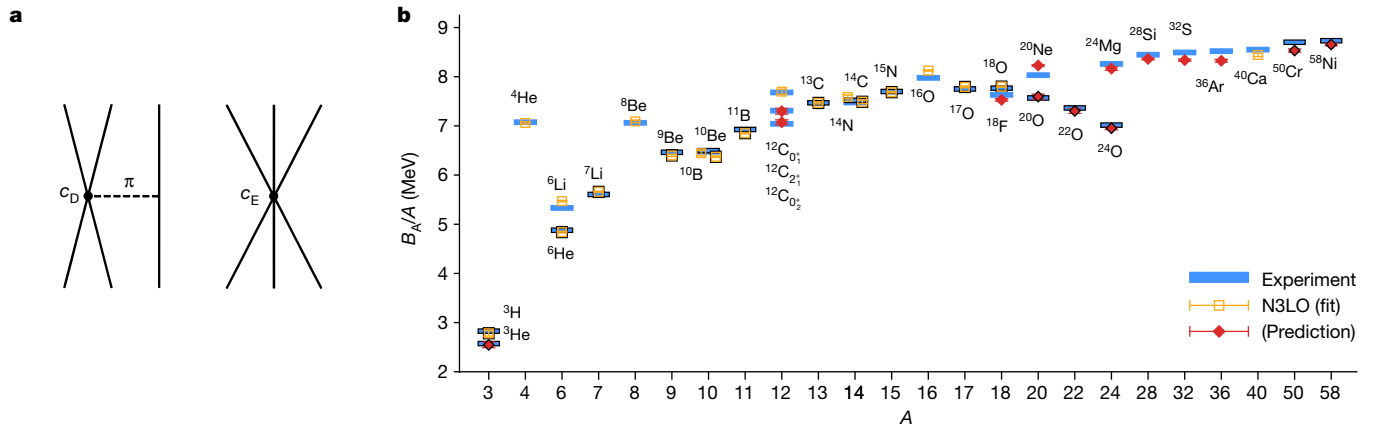
Fig. 2 | Short-range three-nucleon forces at NNLO and results for nuclear binding energies. a, Short-range three-nucleon forces at NNLO. The first is the one-pion exchange term c_D shown on the left. The other is the purely short-range term c_E shown on the right. At order N3LO, there are additional three-nucleon interactions associated with the exchange of two pions, as well as the corrections from the renormalization of the c_D and c_E terms. **b**, Results for nuclear binding energies (B_A) using wavefunction matching. Calculated ground-state and excited-state energies of some selected nuclei with up to $A = 58$ at N3LO in χEFT and comparison with experimental data. The symbols with a black border indicate nuclei with unequal numbers of protons and neutrons. The nuclei used in the fit of the higher-order three-nucleon interactions are labelled with open squares and the other nuclei are predictions denoted with filled diamonds. The error bars show standard deviations.

this error cancellation. We should emphasize that our calculations are full A-body calculations, and cluster effective field theory is only used to diagnose sensitivities to short-distance physics.

In χEFT, three-nucleon forces first appear at order NNLO. These include terms associated with the exchange of two pions and whose coefficients are determined from pion–nucleon scattering. There are also two interactions with singular short-distance properties that must be regulated and the corresponding couplings fitted to empirical data. As shown in Fig. 2a, c_D corresponds to the short-range interaction of two nucleons linked to a third nucleon through the exchange of a pion, and c_E corresponds to the short-range interaction of all three nucleons. At N3LO, there are additional terms associated with the exchange of two pions as well as readjustments of the c_D and c_E coefficients[55–57]. Four-nucleon interactions also appear at N3LO but are not considered in this work.

We tune the short-distance features of the c_D and c_E three-nucleon interactions to minimize errors in the binding energies of selected light and medium-mass nuclei. A total of six additional three-nucleon parameters are adjusted, and in Supplementary Information we present the details of these parameters along with a detailed description of the fitting procedure and the resulting uncertainty. We find that with just one parameter, the root-mean-square-deviation (RMSD) for the energy per nucleon drops from 1.2 MeV down to 0.4 MeV. With the addition of a few additional parameters, the RMSD per nucleon drops further to about 0.1 MeV. These results are consistent with the hypothesis that the α–α interaction has a key role in nuclear binding and that there are several additional cluster interactions that are sensitive to short-distance physics.

In Fig. 2b, we present the results for the nuclear binding energies using wavefunction matching. We show ground-state and excited-state energies of selected nuclei with up to $A = 58$ nucleons and comparison with experimental data. The symbols with a black border indicate nuclei with unequal numbers of protons and neutrons. The nuclei used in the fit of the three-nucleon interactions are labelled with open squares, and the other nuclei are predictions denoted with filled diamonds. The one-standard-deviation error bars shown in Fig. 2 represent uncertainties due to Monte Carlo errors, infinite-volume extrapolations and infinite projection time extrapolations. As described in Supplementary Information, we estimate the additional systematic errors due to truncation of the expansion in powers of $H' − H^s$ to be approximately 0.1 MeV per nucleon. However, this source of systematic error can be

significantly reduced by allowing for variational optimization of the Hamiltonian used to prepare the nuclear many-body wavefunction. We perform this variational optimization so that the remaining systematic error is smaller than the estimated computational error due to other sources. In Supplementary Information, we also compute the additional systematic errors due to uncertainties in the chiral interactions.

In Fig. 3a, we present the results for the charge radii of nuclei with up to $A = 58$ nucleons. No charge radii data were used to fit any interaction parameters. The one-standard-deviation point estimate error bars shown in Fig. 3 represent computational uncertainties due to Monte Carlo errors, infinite-volume extrapolation and infinite-time extrapolation. The agreement with empirical results is quite good, with an RMSD of about 0.03 fm. An extended analysis for selected nuclei that also includes uncertainties from the interactions are presented in Supplementary Information. We note that the larger errors for the heaviest nuclei are statistical and can be decreased by utilizing greater computational resources. The specific terms included in the calculations of the charge radii are detailed in Supplementary Information.

In Fig. 3b, we present lattice results for the energy per nucleon versus density for pure neutron matter and symmetric nuclear matter. None of the neutron-matter and symmetric nuclear-matter data were used to fit any interaction parameters. The density is expressed as a fraction of the saturation density for nuclear matter, $\rho_0 = 0.16$ fm^{-3}. For the neutron-matter calculations, we consider 14 to 80 neutrons in periodic box lengths ranging from 6.58 fm to 13.2 fm. For the symmetric nuclear-matter calculations, we use system sizes from 12 to 160 nucleons in a periodic box of length 9.21 fm. The comparisons with several other published works are shown and detailed in the figure caption. We see that the neutron-matter calculations agree well with previous calculations. Within the uncertainties due to finite system size corrections, the symmetric nuclear-matter calculations show saturation at an energy and density consistent with the empirical saturation point labelled with the black rectangular box. The relative uncertainties due to finite system size are at the 10% level for the energy. Additional calculations with larger systems are needed to reduce the thermodynamic extrapolation error further.

The one-standard-deviation point estimate error bars shown represent computational uncertainties due to Monte Carlo errors and infinite projection time extrapolation. These lattice simulations of symmetric nuclear matter are qualitatively different to other theoretical calculations that assume a homogeneous phase. The lattice
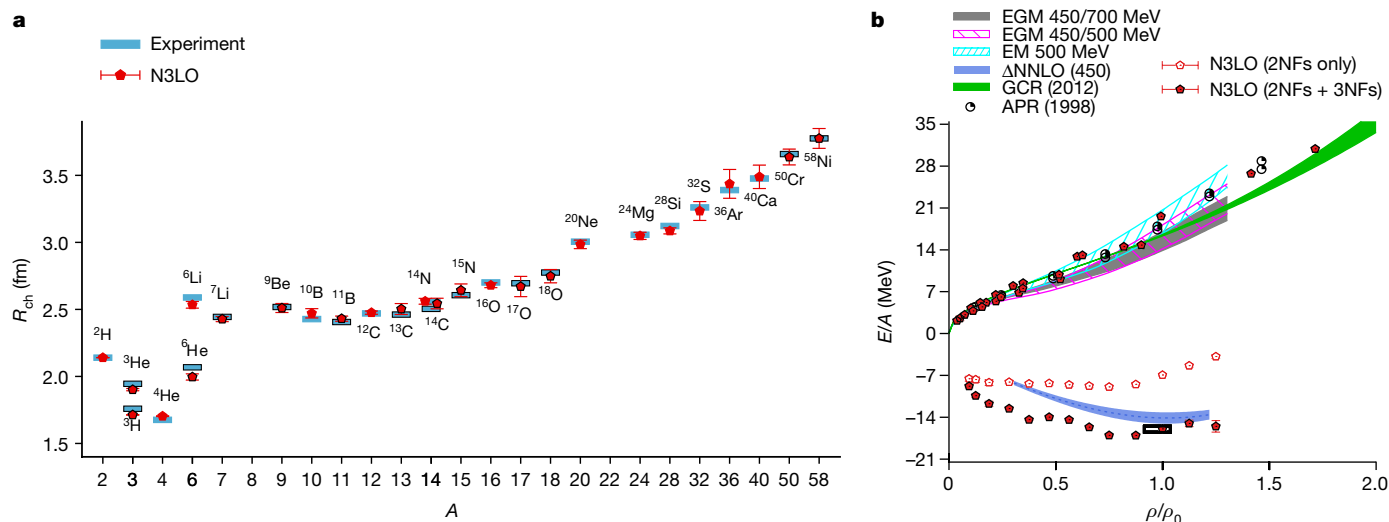
Article

Fig. 3 | Predictions for charge radii of nuclei and for pure neutron-matter energy per neutron and symmetric nuclear-matter energy per nucleon. **a**, Predictions for charge radii (R_{ch}) of nuclei up to $A = 58$ at N3LO in χEFT and comparison with experimental data. The symbols with a black border indicate nuclei with unequal numbers of protons and neutrons. **b**, Predictions for pure neutron-matter energy per neutron and symmetric nuclear-matter energy per nucleon as a function of density at N3LO in χEFT. For pure neutron matter, we use the number of neutrons from 14 to 80 and various box sizes from 6.58 fm to 13.2 fm. For symmetric nuclear matter, we use nucleon numbers from 12 to 160

and a periodic box of length 9.21 fm. For comparison, we show the results from variational calculations (APR)[65], auxiliary-field diffusion Monte Carlo simulations (GCR)[66], many-body perturbation theory using N3LO/NNLO (two-nucleon (2NF)/three-nucleon (3NF)) chiral interactions (EM 500 MeV, EGM 450/500 MeV and EGM 450/700 MeV)[67] and coupled cluster theory using NNLO chiral interactions with explicit delta degrees of freedom (ΔNNLO)[68]. The empirical saturation point is labelled with a black rectangular box. E denotes energy, ρ is the nucleon density, and ρ_0 is the saturation density of symmetric nuclear matter. The error bars show standard deviations.

simulations show phase separation and cluster formation, just as in the real physical system. Owing to the finite number of nucleons in these calculations, some oscillations due to nuclear shell effects can be seen in the energy per nucleon.

Another interesting feature of the lattice results is that symmetric nuclear matter without three-nucleon forces is underbound rather than overbound. This is different from what is found in other calculations using renormalization-group methods[58–60]. As discussed in Supplementary Information, wavefunction matching is very different from renormalization-group transformations. Wavefunction matching implements a unitary transformation that has finite range, and the process can be viewed as defining a new χEFT two-nucleon Hamiltonian H'. The interaction in H' has a range no larger than that of H and H^S for the low-energy interactions. Therefore, one does not need to reconstruct the many-body forces induced by the unitary transformation and can simply treat H' as the new χEFT two-nucleon Hamiltonian. Wavefunction matching has some characteristics similar to the unitary correlation operator method (UCOM)[61–63]. However, the unitary transformation in UCOM has properties that are more similar to renormalization-group transformations and, therefore, is also quite different from wavefunction matching. The induced forces generated by wavefunction matching have been investigated in a toy model[64]. A detailed discussion of the theory and applications of wavefunction matching and its implementation in continuous space are presented in Supplementary Information.

In summary, we have presented an approach for solving quantum many-body systems called wavefunction matching. Wavefunction matching uses a transformation of the particle interactions to allow for calculations of systems that would otherwise be difficult or impossible. We have applied the method to lattice Monte Carlo simulations of light nuclei, medium-mass nuclei, neutron matter and nuclear matter using high-fidelity chiral interactions and found good agreement with empirical data. Judging from the accuracy of the predictions, we have been successful in cancelling systematic errors in nuclear structure calculations by tuning the short-distance features of the three-nucleon

interactions. These developments may help resolve long-standing challenges in ab initio nuclear structure theory.

Although we have focused on Monte Carlo simulations for nuclear physics here, wavefunction matching can be used with any computational method and applied to any quantum many-body system. This also includes quantum computing algorithms where wavefunction matching can be used to reduce the number of quantum gates required. All that is needed is a simple Hamiltonian H^S that produces fair agreement with empirical data for the many-body system of interest and is easily computable using the method of choice. Further details on the implementation and theory of wavefunction matching are given in Supplementary Information.

Online content

Any methods, additional references, Nature Portfolio reporting summaries, source data, extended data, supplementary information, acknowledgements, peer review information; details of author contributions and competing interests; and statements of data and code availability are available at https://doi.org/10.1038/s41586-024-07422-z.

1. Assaad, F. & Evertz, H. in *Computational Many-Particle Physics* (eds Fehske, H., Weiße, A. & Schneider, R.) 277–356 (Springer, 2008).
2. Schollwöck, U. The density-matrix renormalization group in the age of matrix product states. *Ann. Phys.* **326**, 96–192 (2011).
3. Orús, R. A practical introduction to tensor networks: matrix product states and projected entangled pair states. *Ann. Phys.* **349**, 117–158 (2014).
4. Dovesi, R., Civalleri, B., Roetti, C., Saunders, V. R. & Orlando, R. Ab initio quantum simulation in solid state chemistry. *Rev. Comput. Chem.* **21**, 1–125 (2005).
5. Friesner, R. A. Ab initio quantum chemistry: methodology and applications. *Proc. Natl Acad. Sci. USA* **102**, 6648–6653 (2005).
6. Bartlett, R. J. & Musiał, M. Coupled-cluster theory in quantum chemistry. *Rev. Mod. Phys.* **79**, 291 (2007).
7. Aymar, M., Greene, C. H. & Luc-Koenig, E. Multichannel Rydberg spectroscopy of complex atoms. *Rev. Mod. Phys.* **68**, 1015 (1996).
8. Stone, A. & Misquitta, A. Atom–atom potentials from ab initio calculations. *Int. Rev. Phys. Chem.* **26**, 193–222 (2007).
9. Motta, M. & Zhang, S. Ab initio computations of molecular systems by the auxiliary-field quantum Monte Carlo method. *Wiley Interdiscip. Rev. Comput. Mol. Sci.* **8**, e1364 (2018).

10. Barrett, B. R., Navrátil, P. & Vary, J. P. Ab initio no core shell model. *Prog. Part. Nucl. Phys.* **69**, 131–181 (2013).
11. Hagen, G., Papenbrock, T., Hjorth-Jensen, M. & Dean, D. J. Coupled-cluster computations of atomic nuclei. *Rep. Prog. Phys.* **77**, 096302 (2014).
12. Carlson, J. et al. Quantum Monte Carlo methods for nuclear physics. *Rev. Mod. Phys.* **87**, 1067 (2015).
13. Hergert, H., Bogner, S. K., Morris, T. D., Schwenk, A. & Tsukiyama, K. The in-medium similarity renormalization group: a novel ab initio method for nuclei. *Phys. Rep.* **621**, 165–222 (2016).
14. Stroberg, S., Holt, J., Schwenk, A. & Simonis, J. Ab initio limits of atomic nuclei. *Phys. Rev. Lett.* **126**, 022501 (2021).
15. Lee, D. Lattice simulations for few- and many-body systems. *Prog. Part. Nucl. Phys.* **63**, 117–154 (2009).
16. Lähde, T. A. & Meißner, U.-G. *Nuclear Lattice Effective Field Theory: An Introduction* Vol. **975** (Springer, 2019).
17. Epelbaum, E., Hammer, H.-W. & Meißner, U.-G. Modern theory of nuclear forces. *Rev. Mod. Phys.* **81**, 1773–1825 (2009).
18. Machleidt, R. & Entem, D. Chiral effective field theory and nuclear forces. *Phys. Rep.* **503**, 1–75 (2011).
19. Ekström, A. et al. What is ab initio in nuclear theory? *Front. Phys.* **11**, 1129094 (2023).
20. Machleidt, R. What is ab initio? *Few Body Syst.* **64**, 77 (2023).
21. Carlson, J. et al. Quantum Monte Carlo methods for nuclear physics. *Rev. Mod. Phys.* **87**, 1067–1118 (2015).
22. Pastore, S. et al. Quantum Monte Carlo calculations of weak transitions in *A*=6–10 nuclei. *Phys. Rev. C* **97**, 022501 (2018).
23. Gandolfi, S., Lonardoni, D., Lovato, A. & Piarulli, M. Atomic nuclei from quantum Monte Carlo calculations with chiral EFT interactions. *Front. Phys.* **8**, 117 (2020).
24. Lu, B.-N. et al. Essential elements for nuclear binding. *Phys. Lett. B* **797**, 134863 (2019).
25. Lu, B.-N. et al. Ab initio nuclear thermodynamics. *Phys. Rev. Lett.* **125**, 192502 (2020).
26. Shen, S. et al. Emergent geometry and duality in the carbon nucleus. *Nat. Commun.* **14**, 2777 (2023).
27. Gnech, A., Fore, B. & Lovato, A. Distilling the essential elements of nuclear binding via neural-network quantum states. Preprint at https://arxiv.org/abs/2308.16266 (2023).
28. Lu, B.-N. et al. Perturbative quantum Monte Carlo method for nuclear physics. *Phys. Rev. Lett.* **128**, 242501 (2022).
29. Machleidt, R. & Sammarruca, F. Chiral EFT based nuclear forces: achievements and challenges. *Phys. Scr.* **91**, 083007 (2016).
30. Tjon, J. A. Bound states of ⁴He with local interactions. *Phys. Lett. B* **56**, 217–220 (1975).
31. Platter, L., Hammer, H. W. & Meißner, U.-G. On the correlation between the binding energies of the triton and the alpha-particle. *Phys. Lett. B* **607**, 254–258 (2005).
32. Li, N. et al. Neutron–proton scattering with lattice chiral effective field theory at next-to-next-to-next-to-leading order. *Phys. Rev. C* **98**, 044002 (2018).
33. Ekström, A. et al. Accurate nuclear radii and binding energies from a chiral interaction. *Phys. Rev. C* **91**, 051301 (2015).
34. Drischler, C., Hebeler, K. & Schwenk, A. Chiral interactions up to next-to-next-to-next-to-leading order and nuclear saturation. *Phys. Rev. Lett.* **122**, 042501 (2019).
35. Lonardoni, D. et al. Properties of nuclei up to *A*=16 using local chiral interactions. *Phys. Rev. Lett.* **120**, 122502 (2018).
36. Morris, T. D. et al. Structure of the lightest tin isotopes. *Phys. Rev. Lett.* **120**, 152503 (2018).
37. Piarulli, M. et al. Light-nuclei spectra from chiral dynamics. *Phys. Rev. Lett.* **120**, 052503 (2018).
38. Somà, V., Navrátil, P., Raimondi, F., Barbieri, C. & Duguet, T. Novel chiral Hamiltonian and observables in light and medium-mass nuclei. *Phys. Rev. C* **101**, 014318 (2020).
39. Gysbers, P. et al. Discrepancy between experimental and theoretical β-decay rates resolved from first principles. *Nat. Phys.* **15**, 428–431 (2019).
40. Maris, P. et al. Light nuclei with semilocal momentum-space regularized chiral interactions up to third order. *Phys. Rev. C* **103**, 054001 (2021).
41. Hebeler, K. Three-nucleon forces: implementation and applications to atomic nuclei and dense matter. *Phys. Rep.* **890**, 1–116 (2021).
42. Jiang, W. G. et al. Accurate bulk properties of nuclei from *A*=2 to ∞ from potentials with Δ isobars. *Phys. Rev. C* **102**, 054301 (2020).
43. Wirth, R., Yao, J. M. & Hergert, H. Ab initio calculation of the contact operator contribution in the standard mechanism for neutrinoless double beta decay. *Phys. Rev. Lett.* **127**, 242502 (2021).
44. Hu, B. et al. Ab initio predictions link the neutron skin of ²⁰⁸Pb to nuclear forces. *Nat. Phys.* **18**, 1196–1200 (2022).
45. Stroberg, S. R. et al. A nucleus-dependent valence-space approach to nuclear structure. *Phys. Rev. Lett.* **118**, 032502 (2017).
46. Hüther, T., Vobig, K., Hebeler, K., Machleidt, R. & Roth, R. Family of chiral two- plus three-nucleon interactions for accurate nuclear structure studies. *Phys. Lett. B* **808**, 135651 (2020).
47. Hoppe, J., Drischler, C., Hebeler, K., Schwenk, A. & Simonis, J. Probing chiral interactions up to next-to-next-to-next-to-leading order in medium-mass nuclei. *Phys. Rev. C* **100**, 024318 (2019).
48. Nosyk, Y., Entem, D. R. & Machleidt, R. Nucleon–nucleon potentials from Δ-full chiral effective-field-theory and implications. *Phys. Rev. C* **104**, 054001 (2021).
49. Elhatisari, S. et al. Nuclear binding near a quantum phase transition. *Phys. Rev. Lett.* **117**, 132501 (2016).
50. Kanada-En'yo, Y. & Lee, D. Effective interactions between nuclear clusters. *Phys. Rev. C* **103**, 024318 (2021).
51. Bertulani, C. A., Hammer, H. W. & Van Kolck, U. Effective field theory for halo nuclei. *Nucl. Phys. A* **712**, 37–58 (2002).
52. Higa, R., Hammer, H. W. & van Kolck, U. Alpha alpha scattering in halo effective field theory. *Nucl. Phys. A* **809**, 171–188 (2008).
53. Rotureau, J. & van Kolck, U. Effective field theory and the Gamow shell model: the ⁶He halo nucleus. *Few Body Syst.* **54**, 725–735 (2013).
54. Hammer, H. W., Ji, C. & Phillips, D. R. Effective field theory description of halo nuclei. *J. Phys. G* **44**, 103002 (2017).
55. Ishikawa, S. & Robilotta, M. R. Two-pion exchange three-nucleon potential: *O(q⁴)* chiral expansion. *Phys. Rev. C* **76**, 014006 (2007).
56. Bernard, V., Epelbaum, E., Krebs, H. & Meißner, U.-G. Subleading contributions to the chiral three-nucleon force. I. Long-range terms. *Phys. Rev. C* **77**, 064004 (2008).
57. Bernard, V., Epelbaum, E., Krebs, H. & Meißner, U. G. Subleading contributions to the chiral three-nucleon force II: short-range terms and relativistic corrections. *Phys. Rev. C* **84**, 054001 (2011).
58. Bogner, S. K., Kuo, T. T. S., Schwenk, A., Entem, D. R. & Machleidt, R. Towards a model independent low momentum nucleon nucleon interaction. *Phys. Lett. B* **576**, 265–272 (2003).
59. Bogner, S. K., Furnstahl, R. J. & Perry, R. J. Similarity renormalization group for nucleon–nucleon interactions. *Phys. Rev. C* **75**, 061001 (2007).
60. Bogner, S., Furnstahl, R. & Schwenk, A. From low-momentum interactions to nuclear structure. *Prog. Part. Nucl. Phys.* **65**, 94–147 (2010).
61. Feldmeier, H., Neff, T., Roth, R. & Schnack, J. A unitary correlation operator method. *Nucl. Phys. A* **632**, 61–95 (1998).
62. Neff, T. & Feldmeier, H. Tensor correlations in the unitary correlation operator method. *Nucl. Phys. A* **713**, 311–371 (2003).
63. Roth, R., Neff, T. & Feldmeier, H. Nuclear structure in the framework of the unitary correlation operator method. *Prog. Part. Nucl. Phys.* **65**, 50–93 (2010).
64. Bovermann, L., Epelbaum, E., Krebs, H. & Lee, D. Lattice improvement of nuclear shape calculations using unitary transformations. *Proc. Sci.* https://doi.org/10.22323/1.396.0369 (2022).
65. Akmal, A., Pandharipande, V. R. & Ravenhall, D. G. The equation of state of nucleon matter and neutron star structure. *Phys. Rev. C* **58**, 1804–1828 (1998).
66. Gandolfi, S., Carlson, J. & Reddy, S. The maximum mass and radius of neutron stars and the nuclear symmetry energy. *Phys. Rev. C* **85**, 032801 (2012).
67. Tews, I., Krüger, T., Hebeler, K. & Schwenk, A. Neutron matter at next-to-next-to-next-to-leading order in chiral effective field theory. *Phys. Rev. Lett.* **110**, 032504 (2013).
68. Ekström, A., Hagen, G., Morris, T. D., Papenbrock, T. & Schwartz, P. D. Δ isobars and nuclear saturation. *Phys. Rev. C* **97**, 024332 (2018).

Article

Data availability
All of the data produced in association with this work have been stored and are publicly available at https://drive.google.com/drive/folders/1MByuG6NMagcgmURe4py-kwr9vksnHCl4.

Code availability
All of the codes produced in association with this work have been stored and can be obtained upon request from the corresponding author, subject to possible export control constraints.